Linear-in-Complexity Computational Strategies for Modeling and Dosimetry at TeraHertz

Linear-in-Complexity Computational Strategies for Modeling and Dosimetry at TeraHertz

Viviana Giunzioni[(1)], Giuseppe Ciacco[(1)], Clément Henry[(2)], Adrien Merlini[(2)], and Francesco P. Andriulli[(1)]

[(1)] Department of Electronics and Telecommunications, Politecnico di Torino, Italy
[(2)] Microwaves Department, IMT Atlantique, Brest, France

***Abstract*—This work presents a fast direct solver strategy allowing full-wave modeling and dosimetry at terahertz (THz) frequencies. The novel scheme leverages a preconditioned combined field integral equation together with a regularizer for its elliptic spectrum to enable its compression into a non-hierarchical skeleton, invertible in quasi-linear complexity. Numerical results will show the effectiveness of the new scheme in a realistic skin modeling scenario.**

***Index Terms*—integral equations, dosimetry, terahertz, fast solver**

I. Introduction

With the technological advances in THz technology, a growing number of interdisciplinary applications in the THz range have emerged and gained popularity in the last two decades within areas ranging from security, to communications, or biomedicine [1]. As the impact of THz devices in our societies grows, accurately assessing the effects of THz waves on the human body gains crucial importance [2]. Hence the need for exposure analyses that aim at quantifying the amount of energy absorbed by biological tissues subject to electromagnetic radiations [3].

Preliminary dosimetry assessments are a fundamental phase during the design of THz equipments, to guarantee their compliance with the limits on the power absorbed by human tissues set by international agencies [4]. Exposure measurements are often challenging to perform, especially in the near field, but this challenge can be, in part, sidestepped by reliable and accurate numerical dosimetric assessments, when they are within reach. However numerical modeling at THz also comes with its own set of complications.

On the one hand, many of the solvers proposed in the literature employ approximations of the Maxwell's system, suitable to the high frequency regime considered, or apply geometrical simplification to make use of proper analytic solutions. However, application of these approximations can degrade the solution accuracy, and potentially compromise the reliability of the dosimetric analyses. On the other hand, full-wave models leverage the original Maxwell system and can be applied to arbitrarily complex geometries, but the higher computational costs incurred can become prohibitive. In addition, they suffer from numerical issues, such as ill-conditioning or spurious resonances at high frequencies [5] that need to be handled to obtain reliable results.

We propose here a novel full-wave approach, well suited to modeling reflection and absorption of THz waves by biological samples. Being a fast direct solution strategy, this approach allows for the efficient solution of the THz problems for multiple exposures at once, with a complexity which grows only quasi-linearly with the number of unknowns, that is, with increasing frequency. This is obtained by first defining a proper set of boundary integral equations and leveraging a tailored preconditioning scheme, resulting in a well-conditioned system of linear equations freed from spurious resonances. This formulation is then coupled with a recently proposed fast inversion strategy [6], that relies on the compression of the elliptic spectrum of the boundary operator into a rank-deficient skeleton form and on the use of the Woodbury matrix identity [7].

II. Background and Notation

Dosimetry analyzes aim at assessing the amount of energy absorbed by the human body when exposed to an electromagnetic radiation. This estimation can be performed by numerically simulating the response of the biological tissue to the impinging field through a full-wave electromagnetic solver. In this work we employ the two-dimensional approximation, that assumes tha invariance of the geometries and field along an axis $\hat{\boldsymbol{z}}$. This lends itself well to the case under study given the large dimensions of some body parts compared to THz wavelengths. However, this approximation is not suited to modeling all body parts.

Based on the representation theorem [8], different boundary integral equations (BIEs) can be set up to numerically model the time-harmonic electromagnetic scattering and absorption of a penetrable body. Given a two-dimensional domain Ω with boundary $\Gamma \coloneqq \partial\Omega$ characterized by the outgoing normal field $\hat{\boldsymbol{n}}$, the boundary integral operators [8]

$$\left(\mathcal{S}_k^{\Gamma}\psi\right)(\boldsymbol{r}) \coloneqq \int_{\Gamma} G_k(\boldsymbol{r}-\boldsymbol{r}')\psi(\boldsymbol{r}')\mathrm{d}S(\boldsymbol{r}')\,, \tag{1}$$

$$\left(\mathcal{D}_k^{\Gamma}\psi\right)(\boldsymbol{r}) \coloneqq \text{p.v.}\int_{\Gamma} \partial_{\boldsymbol{n}'} G_k(\boldsymbol{r}-\boldsymbol{r}')\psi(\boldsymbol{r}')\mathrm{d}S(\boldsymbol{r}')\,, \tag{2}$$

$$\left(\mathcal{D}_k^{*\Gamma}\psi\right)(\boldsymbol{r}) \coloneqq \text{p.v.}\int_{\Gamma} \partial_{\boldsymbol{n}} G_k(\boldsymbol{r}-\boldsymbol{r}')\psi(\boldsymbol{r}')\mathrm{d}S(\boldsymbol{r}')\,, \tag{3}$$

$$\left(\mathcal{N}_k^{\Gamma}\psi\right)(\boldsymbol{r}) \coloneqq -\text{f.p.}\int_{\Gamma} \partial_{\boldsymbol{n}}\partial_{\boldsymbol{n}'} G_k(\boldsymbol{r}-\boldsymbol{r}')\psi(\boldsymbol{r}')\mathrm{d}S(\boldsymbol{r}')\,, \tag{4}$$

which are respectively the single layer, double layer, adjoint double layer, and hypersingular operator, constitute the building blocks of any of these formulations. The notations p.v. and f.p. indicate the Cauchy principal value and the Hadamard

finite part. We denote by G_k the two-dimensional Green's function in free-space

$$G_k(\boldsymbol{r}-\boldsymbol{r}') = -\frac{j}{4}H_0^{(2)}\left(k||\boldsymbol{r}-\boldsymbol{r}'||\right)\,, \tag{5}$$

where $H_0^{(2)}$ is the Hankel function of the second kind with order zero as defined in [9].

Moreover, numerical exposure assessments also require the *a priori* definition of a realistic model of the tissue under study, both in terms of geometry and dielectric permittivity. Research on THz external dosimetry is often focused on the skin [3], [10], as THz impinging field is absorbed by this organ. Different geometrical models of the skin have been proposed [11] to accurately reproduce the human anatomy. They usually aim at modeling the stratification of compartments with different physical properties, such as the stratum corneum, the epidermis, and the dermis layers, sometimes even modeling anisotropies and depth-varying water percentage [11], at the cost of increasing model complexity. For the sake of simplicity, in this work we employ a single-dielectric model. Following the double Debye model [12], the permittivity of the skin as a function of the frequency is modeled as

$$\epsilon_r(\omega) = \epsilon_\infty + \frac{\epsilon_s-\epsilon_2}{1+j\omega\tau_1} + \frac{\epsilon_2-\epsilon_\infty}{1+j\omega\tau_2}\,, \tag{6}$$

with parameters $\epsilon_\infty = 3$, $\epsilon_s = 60$, $\epsilon_2 = 3.6$, $\tau_1 = 10\,\text{ps}$, and $\tau_2 = 0.2\,\text{ps}$ [13]. The validity of this approximation has been demonstrated in previous works [14], which however have also highlighted a limitation of the model when applied to dry skin and, in general, to tissues characterized by low water contents.

III. Fast Direct Solver Strategy for THz Dosimetry

We propose here a fast direct solver strategy for modeling the electromagnetic response of a biological tissue of boundary Γ_s to an excitation realized by means of a metallic body of boundary Γ_m. It is based on a composite formulation made up of the combined field integral equation (CFIE) for perfect electric conductor (PEC) materials [15] and of the Poggio-Miller-Chang-Harrington-Wu-Tsai (PMCHWT) equation for penetrable media [16]. As is sometimes done in the literature, we assume that the coupling terms between the metallic and the dielectric objects can be neglected [17], [18]. In the case where both objects (i.e., the metallic and the dielectric ones) are subject to a TM polarized field, the resulting system of integral equations is given in eq. (7) at the bottom of the page. Similar results can be found for different polarizations.

In these equations, we denote by the subscript $_0$ the quantities related to the exterior medium, which can be assumed to be the air, and by the subscript $_1$ the ones related to the interior, penetrable, medium. The exterior and interior wavenumbers are denoted as $k_0 = \omega\sqrt{\epsilon_0\mu_0}$ and $k_1 = \omega\sqrt{\epsilon_1\mu_1}$, while $\eta_{0/1} = \sqrt{\mu_{0/1}/\epsilon_{0/1}}$ are the characteristic impedances of the exterior or interior medium. $(E^{\text{inc},m}, H^{\text{inc},m})$ and $(E^{\text{inc},s}, H^{\text{inc},s})$ are the electromagnetic fields incident over Γ_m and Γ_s respectively, further separated into the transversal and longitudinal components, denoted by $_t$ and $_z$. In the following, we will denote by the subscripts $_m$ and $_s$ quantities related to Γ_m and Γ_s respectively.

The unknowns in eq. (7) are the surface equivalent currents defined on the metallic and dielectric boundaries. They are of electric type only in the former case, $j_{z,m}$, and of both electric and magnetic type in the latter, $j_{z,s}$ and $m_{t,s}$. In particular, by superimposing the radiation provided by these currents, it is possible to retrieve the scattered electromagnetic field, to be summed to the incident field in order to determine the resulting electric and magnetic fields everywhere and, in particular, inside the biological sample.

The application of a Galerkin discretization scheme, based on the approximation of the unknown currents as linear combinations of $N_{m/s}$ piecewise linear basis functions $\lambda_i(\boldsymbol{r})$ defined on a mesh of the boundary $\Gamma_{m/s}$, as $j_{z,m/s} \simeq \sum_{i=1}^{N_{m/s}}(\boldsymbol{j}_{z,m/s})_i\lambda_i$ and $m_{t,s} \simeq \sum_{i=1}^{N_{m/s}}(\boldsymbol{m}_{t,s})_i\lambda_i$, results in the linear system of equations

$$\begin{pmatrix} \boldsymbol{C} & \mathsf{o} & \mathsf{o} \\ \mathsf{o} & \boldsymbol{P}_{11} & \boldsymbol{P}_{12} \\ \mathsf{o} & \boldsymbol{P}_{21} & \boldsymbol{P}_{22} \end{pmatrix} \begin{pmatrix} \boldsymbol{j}_{z,m} \\ \boldsymbol{j}_{z,s} \\ \boldsymbol{m}_{t,s} \end{pmatrix} = \begin{pmatrix} \boldsymbol{e}_{z,m}/(jk_0\eta_0) + \boldsymbol{h}_{t,m} \\ \boldsymbol{e}_{z,s} \\ \boldsymbol{h}_{t,s} \end{pmatrix}. \tag{8}$$

In the above system,

$$(\boldsymbol{e}_{z,m/s})_i = \left(\lambda_i, E_z^{\text{inc},m/s}\right)_{L^2(\Gamma_{s/m})} \tag{9}$$

$$(\boldsymbol{h}_{t,m/s})_i = \left(\lambda_i, H_t^{\text{inc},m/s}\right)_{L^2(\Gamma_{s/m})}\,, \tag{10}$$

and the matrices $\boldsymbol{C}$, $\boldsymbol{P}_{11}$, $\boldsymbol{P}_{12}$, $\boldsymbol{P}_{21}$, and $\boldsymbol{P}_{22}$ are defined as

$$\boldsymbol{C} = \boldsymbol{S}_{k_0}^{\Gamma_m} + \frac{1}{2}\boldsymbol{G}^{\Gamma_m} + \boldsymbol{D}_{k_0}^{*\Gamma_m} \tag{11}$$

$$\boldsymbol{P}_{11} = -jk_0\eta_0\boldsymbol{S}_{k_0}^{\Gamma_s} - jk_1\eta_1\boldsymbol{S}_{k_1}^{\Gamma_s} \tag{12}$$

$$\boldsymbol{P}_{12} = \boldsymbol{D}_{k_0}^{\Gamma_s} + \boldsymbol{D}_{k_1}^{\Gamma_s} \tag{13}$$

$$\boldsymbol{P}_{21} = -\left(\boldsymbol{D}_{k_0}^{*\Gamma_s} + \boldsymbol{D}_{k_1}^{*\Gamma_s}\right) \tag{14}$$

$$\boldsymbol{P}_{22} = -1/(jk_0\eta_0)\boldsymbol{N}_{k_0}^{\Gamma_s} - 1/(jk_1\eta_1)\boldsymbol{N}_{k_1}^{\Gamma_s}\,, \tag{15}$$

where we have used the generic notation $(\boldsymbol{O}_k^\Gamma)_i j = \left(\lambda_i, O_k^\Gamma\lambda_j\right)_{L^2(\Gamma)}$, where O stands for one of $\{\mathcal{S}, \mathcal{D}, \mathcal{D}^*, \mathcal{N}\}$. The gram matrix $\boldsymbol{G}^\Gamma$ is obtained as $(\boldsymbol{G}^\Gamma)_{ij} = (\lambda_i, \lambda_j)_{L^2(\Gamma)}$.

$$\begin{cases} \mathcal{S}_{k_0}^{\Gamma_m} j_{z,m}(\boldsymbol{r}) + \left(\frac{1}{2}\mathcal{I} + \mathcal{D}_{k_0}^{*\Gamma_m}\right) j_{z,m}(\boldsymbol{r}) = \frac{1}{jk_0\eta} E_z^{\text{inc},m}(\boldsymbol{r}) + H_t^{\text{inc},m}(\boldsymbol{r}), & \boldsymbol{r}\in\Gamma_m \\ \left(-jk_0\eta_0\mathcal{S}_{k_0}^{\Gamma_s} - jk_1\eta_1\mathcal{S}_{k_1}^{\Gamma_s}\right) j_{z,s}(\boldsymbol{r}) + \left(\mathcal{D}_{k_0}^{\Gamma_s} + \mathcal{D}_{k_1}^{\Gamma_s}\right) m_{t,s}(\boldsymbol{r}) = E_z^{\text{inc},s}(\boldsymbol{r}), & \boldsymbol{r}\in\Gamma_s \\ -\left(\mathcal{D}_{k_0}^{*\Gamma_s} + \mathcal{D}_{k_1}^{*\Gamma_s}\right) j_{z,s}(\boldsymbol{r}) + \left(-1/(jk_0\eta_0)\mathcal{N}_{k_0}^{\Gamma_s} - 1/(jk_1\eta_1)\mathcal{N}_{k_1}^{\Gamma_s}\right) m_{t,s}(\boldsymbol{r}) = H_t^{\text{inc},s}(\boldsymbol{r}), & \boldsymbol{r}\in\Gamma_s \end{cases} \tag{7}$$

As a consequence of the fact that the metallic radiator is electrically much larger than the biological sample under study, a significantly higher number of basis functions is required for the discretization of the unknown currents on its boundary Γ_m (following the Nyquist sampling principle). Hence, we infer that the numerical solution of the linear system resulting from the discretization of the CFIE is the bottleneck, in terms of time and memory required, towards the solution of the entire system (8), both directly or iteratively. To alleviate this computational burden, we propose here to extend the Calderón preconditioned scheme presented in [6], [19] for $\boldsymbol{C}$ and to extend the fast direct solver tailored for the resulting well-conditioned operator recently proposed in [6]. In particular, we define the Calderón stabilized operator matrix as

$$\boldsymbol{C}_p := \boldsymbol{N}_{\tilde{k}_0}^{\Gamma_m} \left(\boldsymbol{G}^{\Gamma_m}\right)^{-1} \boldsymbol{S}_{k_0}^{\Gamma_m} + \left(\frac{1}{2}\boldsymbol{G}^{\Gamma_m} - \boldsymbol{D}_{\tilde{k}_0}^{*\Gamma_m}\right) \left(\boldsymbol{G}^{\Gamma_m}\right)^{-1} \left(\frac{1}{2}\boldsymbol{G}^{\Gamma_m} + \boldsymbol{D}_{k_0}^{*\Gamma_m}\right) \tag{16}$$

where, following the approach introduced in [20], $\tilde{k}_0 := k_0 - j0.4k_0^{1/3}a^{-2/3}$, with a evaluated as a suitable average of the radius of curvature along Γ_m. Then, following the procedure described in [6], we express $\boldsymbol{C}_p$ as the sum $\boldsymbol{C}_p = \boldsymbol{C}_{p,\mathrm{c}} + \boldsymbol{C}_{p,\mathrm{ext}}$, where $\boldsymbol{C}_{p,\mathrm{c}}$ is the circular counterpart of $\boldsymbol{C}_p$ discretized over an equi-perimeter circular boundary. We employ at this point an adaptive randomized algorithm, such as the one presented in [21], to compute a skeleton form of $\boldsymbol{C}_{p,\mathrm{ext}}$ as

$$\boldsymbol{C}_{p,\mathrm{ext}} = \boldsymbol{C}_p - \boldsymbol{C}_{p,\mathrm{c}} \simeq \boldsymbol{U}\boldsymbol{V}^{\mathrm{T}}. \tag{17}$$

Given the spectral properties of matrix $\boldsymbol{C}_{p,\mathrm{ext}}$, the rank of the skeleton $\boldsymbol{U}\boldsymbol{V}^{\mathrm{T}}$ grows only approximately as $k_0^{1/3}$ toward the high frequency limit. As a consequence, by applying a proper acceleration technique such as the fast multiple method (FMM) [22], the solution of the system, for any number of right hand sides, can be obtained efficiently, in quasi-linear complexity, by directly evaluating the inverse [7]

$$\boldsymbol{C}_p^{-1} = \boldsymbol{C}_{p,\mathrm{c}}^{-1} - \boldsymbol{C}_{p,\mathrm{c}}^{-1}\boldsymbol{U}\left(\boldsymbol{I} + \boldsymbol{V}^{\mathrm{T}}\boldsymbol{C}_{p,\mathrm{c}}^{-1}\boldsymbol{U}\right)^{-1}\boldsymbol{V}^{\mathrm{T}}\boldsymbol{C}_{p,\mathrm{c}}^{-1}. \tag{18}$$

In particular, after noticing that all operations involving circulant matrices are computed rapidly via the use of the fast Fourier transform (FFT) algorithm, we recognize that the complexity of evaluating (18) scales in frequency approximately as $k_0^{4/3}$, with an overhead complexity with respect to the linear one determined by the skeleton rank increase.

IV. Numerical results

In this section, we first aim at assessing the efficiency of the fast direct solver. The rank of the skeleton form $\boldsymbol{U}\boldsymbol{V}^{\mathrm{T}}$ is the key parameter to observe, as it directly determines the computational complexity of the method, affecting both time and memory required. The first geometry analyzed is the ellipse. Figure 1 shows the rank of the skeleton of the operator, for both TE and TM formulations, evaluated over an ellipse with aspect ratio 1.5 and perimeter 2π m. Secondarily,

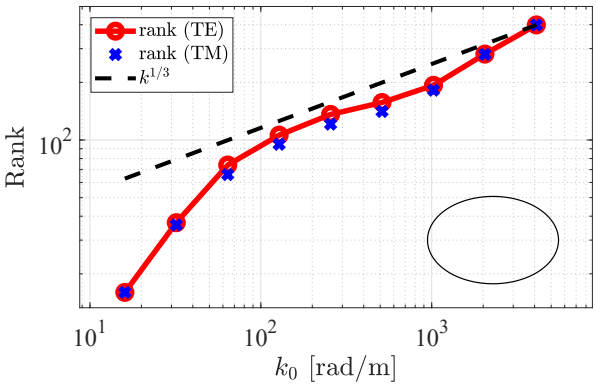

Fig. 1 Rank of the skeleton form $\boldsymbol{U}\boldsymbol{V}^{\mathrm{T}}$ evaluated over an ellipse with aspect ratio 1.5 and perimeter 2π m as a function of the free-space wavenumber k_0.

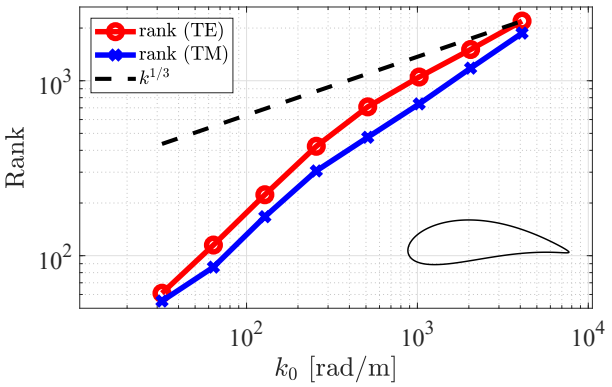

Fig. 2 Rank of the skeleton form $\boldsymbol{U}\boldsymbol{V}^{\mathrm{T}}$ evaluated over an airfoil with perimeter 2π m as a function of the free-space wavenumber k_0.

we have considered an airfoil geometry, resulting from the application of the Joukowsky conformal mapping from the circle, with perimeter 2π m (fig. 2). In both cases, we observe that the rank grows less than linearly with frequency and tends to stabilize to the expected behaviour of $k_0^{1/3}$ in the high frequency limit. Consistently, the compression time (i.e., the time required for the skeleton evaluation), dominating the overall inversion time, scales quasi-linearly, as shown in table I.

Then, we applied the solver to the evaluation of the electromagnetic scattering from a skin sample (fig. 3). In particular, we considered an ellipse of perimeter approximately of 5.85 mm excited by a time-harmonic field at the frequency of 1 THz. We employed the double Debye model (eq. (6)) to approximate the permittivity of the skin, corresponding to a penetration length of approximately 62 µm.

V. Conclusion

This paper presented a fast direct solver strategy for full-wave modeling and dosimetry at terahertz frequencies. This has been obtained by leveraging a preconditioned version of the combined field integral equation, free of spurious high-

N	k_0 [rad/m]	compr. time [s]	eri
15011	833.91	59.33	-
30021	1667.8	129.6	1.13
45032	2501.7	210.2	1.19

Tab. I Compression time required to evaluate the skeleton form $\boldsymbol{UV}^{\mathrm{T}}$ evaluated over an ellipse with aspect ratio 1.5 and perimeter 2π m at different frequencies, corresponding to different numbers of unknowns N, and experimental rate of increase (eri). The simulations have been performed on 25 parallel processes.

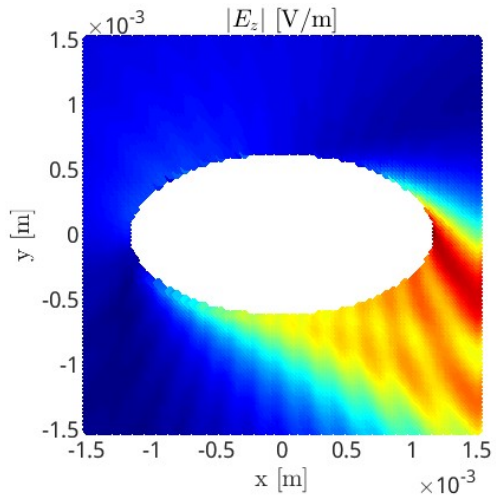

Fig. 3 Magnitude of the longitudinal electric field scattered by the skin given a TM plane-wave excitation at the frequency of 1 THz impinging at an angle of $-1/5\pi$.

frequency resonances, and a suitable compression technique for its elliptic spectrum, resulting in an operator matrix invertible in quasi-linear complexity. The direct nature of the solver makes its use convenient to solve multiple sources problems, where the scatterer response to many different exposures should be analyzed, as it can be the case in dosimetry studies.

Acknowledgment

The work of this paper has received funding from the European Research Council (ERC) under the European Union's Horizon 2020 research and innovation programme (grant agreement No 724846, project 321), from the Horizon Europe Research and innovation programme under the EIC Pathfinder grant agreement n° 101046748 (project CEREBRO), and from the ANR Labex CominLabs under the project "CYCLE".

References

[1] X. Chen, H. Lindley-Hatcher, R. Stantchev, J. Wang, K. Li, A. Hernandez Serrano, Z. Taylor, E. Castro-Camus, and E. Pickwell-MacPherson, "Terahertz (THz) biophotonics technology: Instrumentation, techniques, and biomedical applications," *Chemical Physics Reviews*, vol. 3, no. 1, p. 011311, Mar. 2022.

[2] O. P. Cherkasova, D. S. Serdyukov, A. S. Ratushnyak, E. F. Nemova, E. N. Kozlov, Yu. V. Shidlovskii, K. I. Zaytsev, and V. V. Tuchin, "Effects of terahertz radiation on living cells: A review," *Optics and Spectroscopy*, vol. 128, no. 6, pp. 855–866, Jun. 2020.

[3] S. Alekseev, A. Radzievsky, M. Logani, and M. Ziskin, "Millimeter wave dosimetry of human skin," *Bioelectromagnetics*, vol. 29, no. 1, pp. 65–70, Jan. 2008.

[4] ICNIRP, "Guidelines for limiting exposure to electromagnetic fields (100 kHz to 300 GHz)," *Health Physics*, vol. 118, no. 5, pp. 483–524, May 2020.

[5] S. Adrian, A. Dely, D. Consoli, A. Merlini, and F. Andriulli, "Electromagnetic integral equations: Insights in conditioning and preconditioning," *IEEE Open Journal of Antennas and Propagation*, vol. 2, pp. 1143–1174, 2021.

[6] D. Consoli, C. Henry, A. Dély, L. Rahmouni, J. Ortiz G., T. Chhim, S. Adrian, A. Merlini, and F. Andriulli, "On the fast direct solution of a preconditioned electromagnetic integral equation," Apr. 2022.

[7] H. V. Henderson and S. R. Searle, "On deriving the inverse of a sum of matrices," *SIAM Review*, vol. 23, no. 1, pp. 53–60, Jan. 1981.

[8] J. Nédélec, *Acoustic and Electromagnetic Equations*, ser. Applied Mathematical Sciences, J. E. Marsden and L. Sirovich, Eds. New York, NY: Springer New York, 2001, vol. 144.

[9] F. W. J. Olver and National Institute of Standards and Technology, Eds., *NIST Handbook of Mathematical Functions*. Cambridge: Cambridge Univ. Press [u.a.], 2010.

[10] Z. Haider, Y. Le Drean, G. Sacco, D. Nikolayev, R. Sauleau, and M. Zhadobov, "High-resolution model of human skin appendages for electromagnetic dosimetry at millimeter waves," *IEEE Journal of Microwaves*, vol. 2, no. 1, pp. 214–227, Jan. 2022.

[11] J. Wang, H. Lindley-Hatcher, X. Chen, and E. Pickwell-MacPherson, "THz sensing of human skin: A review of skin modeling approaches," *Sensors*, vol. 21, no. 11, p. 3624, May 2021.

[12] J. T. Kindt and C. A. Schmuttenmaer, "Far-infrared dielectric properties of polar liquids probed by femtosecond terahertz pulse spectroscopy," *The Journal of Physical Chemistry*, vol. 100, no. 24, pp. 10 373–10 379, Jan. 1996.

[13] E. Pickwell, B. E. Cole, A. J. Fitzgerald, V. P. Wallace, and M. Pepper, "Simulation of terahertz pulse propagation in biological systems," *Applied Physics Letters*, vol. 84, no. 12, pp. 2190–2192, Mar. 2004.

[14] E. Pickwell, B. E. Cole, A. J. Fitzgerald, M. Pepper, and V. P. Wallace, "*In Vivo* study of human skin using pulsed terahertz radiation," *Physics in Medicine and Biology*, vol. 49, no. 9, pp. 1595–1607, May 2004.

[15] J. Mavtz and R. Harrington, "H-field, E-field, and combined field solutions for conducting body of revolution," *Archiv Elektronik Übertragungstechnik*, vol. 32, pp. 157–164, 1978.

[16] A. Poggio and E. Miller, "Integral equation solutions of three-dimensional scattering problems," in *Computer Techniques for Electromagnetics*. Elsevier, 1973, pp. 159–264.

[17] M. Ziane, R. Sauleau, and M. Zhadobov, "Antenna/body coupling in the near-field at 60 GHz: Impact on the absorbed power density," *Applied Sciences*, vol. 10, no. 21, p. 7392, Oct. 2020.

[18] G. Sacco, D. Nikolayev, R. Sauleau, and M. Zhadobov, "Antenna/human body coupling in 5G millimeter-wave bands: Do age and clothing matter?" *IEEE Journal of Microwaves*, vol. 1, no. 2, pp. 593–600, Apr. 2021.

[19] F. Andriulli, I. Bogaert, and K. Cools, "On the high frequency behavior and stabilization of a preconditioned and resonance-free formulation," in *2015 International Conference on Electromagnetics in Advanced Applications (ICEAA)*. Torino, Italy: IEEE, Sep. 2015, pp. 1321–1324.

[20] M. Darbas, "Generalized combined field integral equations for the iterative solution of the three-dimensional Maxwell equations," *Applied Mathematics Letters*, vol. 19, no. 8, pp. 834–839, Aug. 2006.

[21] N. Halko, P. G. Martinsson, and J. A. Tropp, "Finding structure with randomness: Probabilistic algorithms for constructing approximate matrix decompositions," *SIAM Review*, vol. 53, no. 2, pp. 217–288, Jan. 2011.

[22] R. Coifman, V. Rokhlin, and S. Wandzura, "The fast multipole method for the wave equation: A pedestrian prescription," *IEEE Antennas and Propagation Magazine*, vol. 35, no. 3, pp. 7–12, Jun. 1993.